Effect of Different Reinforcement Methods on the Flexural Performance of Glued Laminated Timber Beams

Yaoyao Du,* Biqing Shu, Chen Li, Xudong Zhu, and Xuewen Zhang

Glued laminated timber beams are vulnerable to brittle tensile failure in the tension zone, which limits their flexural efficiency and application in modern timber structures. This study investigated two reinforcement strategies for such beams: external steel reinforcement and bottom steel plate reinforcement connected with self-tapping screws. Unreinforced beams were tested as controls. Full-scale four-point bending tests were conducted to evaluate failure mode, load-deflection response, load-strain behaviour, bearing capacity, stiffness, and ductility. A three-dimensional finite element model was then developed and validated against the experimental results. The control beams failed in brittle tension, with an average ultimate load of 21.6 kN. The externally reinforced beams showed no effective improvement in flexural behaviour because prestress transfer and steel-timber interaction were insufficient. In contrast, the steel plate reinforcement restored 76% of the original load-bearing capacity of damaged beams and improved deformation capacity, although failure was still governed by timber delamination and screw shear. The validated numerical model reproduced the full loading-to-failure process and can support the design and optimization of reinforced timber members.

DOI: 10.15376/biores.21.3.7220-7246

Keywords: Glulam beams; Flexural performance; Steel reinforcement; Failure mode; Finite element modeling

*Contact information: School of Civil Engineering and Transportation, Yangzhou Polytechnic Institute, Yangzhou 225127, China; *Corresponding author: 1569864882@qq.com*

INTRODUCTION

The transition of the construction industry towards a green economy has become an irreversible trend within the global macro-strategic framework. This is due to the need to address climate change and advance sustainable development (Tam *et al.* 2017). In order to achieve the strategic objectives of “carbon peaking and carbon neutrality,” the construction sector is compelled to move away from its conventional model, which is characterised by high energy consumption and high greenhouse gas emissions. This transition necessitates a fundamental shift toward low-carbon, environmentally friendly, and energy-efficient construction practices. In the context of the construction industry, timber is being re-evaluated and increasingly recognised for its critical value. This is because timber is a natural, renewable, bio-based material with significant carbon sequestration capacity. It is evident that timber structures satisfy the fundamental criteria for sustainability by virtue of their superior ecological performance. Moreover, they are commensurate with contemporary aspirations for green and healthy living environments. The inherent natural affinity of these materials, in conjunction with their ability to create comfortable indoor spaces and their excellent physical and mechanical properties, serves to further enhance their appeal (De Araujo 2023; Wang *et al.* 2024a). Among various engineered wood products, glued laminated timber (Glulam) occupies a central role in modern timber construction. The primary factors contributing to this phenomenon are its high material efficiency, stringent quality control measures, adaptable dimensional design capabilities, and exceptional mechanical strength. Glulam is particularly well-suited for large-span, expansive, and architecturally complex projects (Shu *et al.* 2020; Zhao *et al.* 2024; Liu *et al.* 2025). Such projects include, but are not limited to, stadiums, convention centers, transportation hubs, and cultural landmarks. Glulam offers important advantages and considerable application potential in such projects.

The mechanical performance of glulam beams is of particular significance within the context of timber structural systems, given its role as the most crucial bending element. Nevertheless, the mechanical behaviour of glulam beams is subject to certain intrinsic limitations. Although the tensile strength parallel to grain of small clear wood specimens may exceed the compressive strength parallel to grain, tensile failure of glulam beams in bending is typically brittle and is highly sensitive to knots, finger joints, local defects, lamination interfaces, and size effects. Consequently, flexural failure in glulam beams often initiates in the tension zone on the underside of the beam, where localized tensile rupture or splitting can develop suddenly (Yang *et al.* 2016b). Such failures often occur without noticeable warning, presenting a significant risk to structural safety. Moreover, prevailing design standards stipulate that the deflection of glulam beams must adhere to serviceability limit state criteria. Consequently, the design of glulam beams is predominantly governed by deformation control, or stiffness control (GB/T 50708 2012; EN 14080 2013). This design philosophy frequently results in the selection of cross-sectional dimensions that exceed the requirements based solely on load-bearing capacity calculations. Consequently, the high compressive strength of the timber in the upper compression zone is largely underutilised. This not only constitutes a considerable inefficiency in terms of material properties, but it also restricts the economic feasibility and broader application of glulam in structures with larger spans. Given the increasing demand in modern architecture for greater spatial spans, addressing key technical challenges has become imperative. These include enhancing the bending load-bearing capacity of glulam beams, improving their failure modes to avoid sudden brittle fractures, and optimizing the utilization efficiency of the cross-sectional area. Achieving these advancements is essential for overcoming current limitations and realizing the full potential of glulam in advanced timber engineering applications (Yang *et al.* 2016a; Wang *et al.* 2024b; Li *et al.* 2025).

To address the inadequate tensile performance at the bottom of glulam beams and the associated risk of brittle failure, researchers have undertaken extensive and pioneering studies, introducing a variety of structural reinforcement and strengthening methodologies. Among these approaches, fibre-reinforced polymer (FRP) reinforcement technology has emerged as the most extensively utilized and rigorously investigated method, because of its outstanding mechanical properties. There is a substantial body of experimental evidence (Gunasekaran *et al.* 2026) that attests to the efficacy of bonded composite materials when applied to the tension zone surface of glulam beams. This efficacy is further compounded by the incorporation of carbon fibre reinforced polymer (CFRP) (Fossetti *et al.* 2015; Glišović *et al.* 2016; He *et al.* 2022; Karagöz İşleyen *et al.* 2023), glass fibre reinforced polymer (GFRP) (Guan *et al.* 2005; Raftery and Whelan 2014; Thorhallsson *et al.* 2017), and fabrics (Uzel *et al.* 2018; Di *et al.* 2023) embedded within the tension zone. These measures have been shown to result in a substantial enhancement of the flexural strength of beams, stiffness, and deformation capacity. These polymer-based composites offer notable advantages, such as low weight, high tensile strength, and superior durability, while also establishing an effective synergistic stress transfer mechanism with the wooden matrix. In addition to FRP-based techniques, steel reinforcement strategies have also proven to be highly effective (De Luca *et al.* 2012; Soriano *et al.* 2016). Conventional approaches, including the embedding of steel rebars or the bonding of steel plates within the tension zone, not only facilitate a more uniform distribution of tensile stresses but also significantly enhance the overall ultimate load-carrying capacity of the structure. These methods concurrently improve the ductility of the beam, shifting the failure mode away from the typically brittle fracture characteristic of wood to a more controlled and predictable sequence: initial yielding of the steel reinforcement, followed by compressive failure of the wood (Kliger *et al.* 2007). Further notable advancements in this field include the integration of high-strength compressed timber elements during the lamination process (Anshari *et al.* 2012; Anshari *et al.* 2017), as well as the development of hybrid reinforcement systems that capitalize on the synergistic effects between steel or concrete and composite materials (Ferrier *et al.* 2012). These multifaceted technical strategies work together to optimize the mechanical performance of glulam beams across various structural dimensions. Collectively, these research findings not only contribute to the refinement of structural design theories specific to glulam beams but also offer dependable engineering guidelines for their practical application. They unequivocally demonstrate the technical viability and real-world applicability of mitigating the inherent tensile limitations of timber through the use of external reinforcement methods.

While the reinforcement methods discussed above have demonstrated substantial improvements in the performance of glulam beams, a more detailed examination of their timing and application contexts reveals that these techniques can be broadly classified into two conceptual categories: “design-stage integrated reinforcement” (or “pre-failure reinforcement”) and “post-construction remedial reinforcement” (or “post-failure reinforcement”). Each category presents unique technical challenges and practical limitations during implementation. The concept of “integrated reinforcement” entails the incorporation of reinforcement materials, such as steel bars or FRP rods, within the wood laminations during the design and manufacturing phases of glulam beams. This process effectively bonds the reinforcement materials into a cohesive structural element, thereby enhancing the overall strength and durability of the glulam beams. The efficacy of this approach is predicated on the robust and integral connection between the reinforcement and the timber substrate, thereby facilitating clear and efficient load transfer pathways that optimise the synergistic interaction among all components. However, it is important to note that this approach is not without significant technical challenges. Firstly, it is important to consider the differential deformation characteristics of reinforcement materials (steel, FRP) and wood under varying temperature and moisture conditions. This includes thermal expansion and contraction, as well as hygroscopic swelling and shrinkage. It is notable that such conditions can induce significant interfacial stresses. It is hypothesised that, over time, these stresses may result in the formation of cracks in the adhesive layer or delamination at the interface. This, in turn, could potentially compromise the long-term structural durability of the material (Chen *et al.* 2022). Secondly, the manufacturing process is inherently more complex, demanding higher precision and reliability from production equipment and stringent quality control systems. This, in turn, raises production costs and increases technical implementation challenges. Thirdly, due to the reinforcement being incorporated during the initial fabrication stage, subsequent modifications or replacements of the internal reinforcement scheme are rendered largely impractical. This has a detrimental effect on design adaptability and future retrofit options. Conversely, the term "retrofit reinforcement" is employed to denote the process of augmenting the structural integrity of existing or damaged structures through the external application of methods, such as the adhesion of FRP fabrics or steel plates to the surface. These techniques offer considerable flexibility, enabling tailored solutions based on specific structural conditions and observed damage.

The purpose of this study was not to demonstrate that the proposed reinforcement schemes outperform well-developed bonded FRP or embedded steel-reinforcement systems. Rather, the study evaluated two practical and easily fabricated reinforcement/ repair configurations and identified their effectiveness and limitations. This study employed a combined experimental and numerical simulation approach. Full-scale four-point bending tests were designed and conducted, using unreinforced glued laminated timber beams as the control group. A systematic analysis was conducted to assess the damage evolution, ultimate failure modes, load-deformation/strain responses, and core mechanical properties of glulam beams under both reinforcement methods. This analysis encompassed a comprehensive range of parameters, including load-carrying capacity, stiffness, and ductility. The testing process involved rigorous and systematic testing to ensure the reliability of the results. Concurrently, a three-dimensional refined finite element model validated by experiments was established to deeply reveal the internal stress distribution and load transfer mechanisms within glulam beams under different reinforcement schemes. This study aimed to quantitatively evaluate the enhancement and restoration efficacy of the two reinforcement methods on the mechanical properties of glulam beams, elucidate their reinforcement principles, and identify technical limitations. It provided experimental evidence for future optimization and validation.

EXPERIMENTAL

Material Properties

This experiment used Douglas fir as the glulam species of choice. The glulam timber used in the study had a smooth, flat surface with no noticeable defects or imperfections. It demonstrated notable mechanical properties, including high hardness and strength, as well as excellent dimensional stability and strong corrosion resistance. To ensure a standardised evaluation, the density and moisture content of wood were measured in accordance with Chinese national standards (GB/T 1927.5 2021) and (GB/T 1927.4 2021), respectively. For mechanical testing, a series of specimens were prepared in accordance with the relevant standards. All test specimens were prepared in six copies. Different specimen geometries were used because the compression-strength test and the modulus-of-elasticity test follow different Chinese standards and require different gauge lengths and loading configurations. The 30 mm × 20 mm × 20 mm specimens were used for compression strength parallel to grain according to GB/T 1927.11 (2022), whereas the 60 mm × 20 mm × 20 mm specimen was used for modulus-of-elasticity measurement according to GB/T 15777 (2017), which provides a longer gauge length for deformation measurement. All specimens were cut from the same Douglas fir glulam batch and aligned with the longitudinal grain direction to minimize material variability. Tensile strength parallel to grain was determined according to GB/T 1927.14 (2022). Figure 1 shows the exact dimensions of all prepared specimens and the testing equipment used. The detailed test results regarding the mechanical properties of the wood are presented in Table 1.

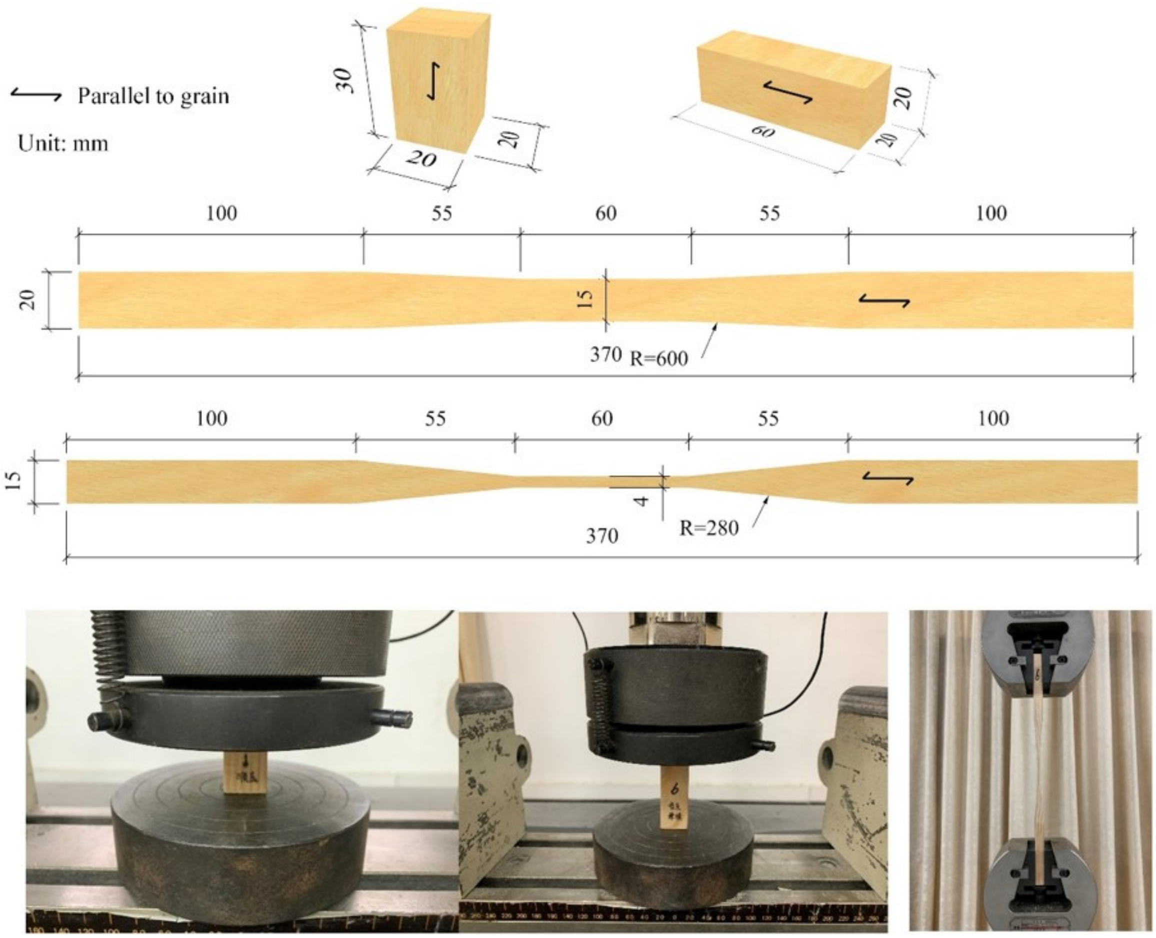

Fig. 1. Geometric parameters and test diagram for material properties testing

Table 1. Wood Properties

Properties	Values (CoV)
Modulus of elasticity (MPa)	9096 (2.3%)
Compressive strength (MPa)	36.0 (2.4%)
Tensile strength (MPa)	85.5 (9.7%)
Density (kg/m^3)	540 (2.9%)
Moisture content (%)	10.5 (6.8%)

Notes: CoV = Coefficient of variation

The bolts utilized in this study were hexagon head bolts with a strength grade of 8.8, characterized by a nominal diameter of 8 mm and a total length of 80 mm. The steel plates were fabricated from Q345 grade structural steel. For fastening, TP30 double countersunk self-drilling wood screws, supplied by Shanghai Meigu Chengfan Fastener Co., Ltd., were employed; these screws feature an internal thread diameter of 4 mm and a length of 60 mm. The mechanical properties of all steel components were assessed in accordance with the procedures specified in the national standard GB/T 228.1 (2022). The 8.8-grade high-strength structural bolts demonstrate a yield strength of 635 MPa and an ultimate tensile strength of 840 MPa. For the TP30 screws and Q345B steel plates, both materials possess an identical modulus of elasticity of 210,000 MPa. Their respective yield strengths are 489 MPa for the TP30 screws and 463 MPa for the Q345B steel plates, while the ultimate tensile strengths are 610 MPa for the TP30 screws and 664 MPa for the Q345B steel plates.

Specimens Preparation

The study systematically investigated the impact of two reinforcement techniques for enhancing the flexural capacity of glulam beams. The reinforcement techniques in question were external steel reinforcement and bottom steel plate reinforcement. Three specimen groups were designed and fabricated for testing: the control group comprised ordinary glulam beams (A1 to A3); the second group consisted of externally reinforced glulam beams (B1 to B3); and the third group included steel plate-reinforced glulam beams (C1 to C3). To maintain uniform testing conditions, the span-to-depth ratio of all beams was kept within the range 1/12 to 1/18. All beam specimens were fabricated with identical cross-sectional dimensions: 1800 mm in length, 60 mm in width, and 100 mm in height. The source specimens used for the C-series beams were tracked during the retrofit process. Specimen C1 was prepared from the previously failed specimen A1, C2 from A2, and C3 from A3. No separate destructive residual-capacity test was conducted before retrofitting, because additional loading would have further altered the damage state of the already failed beams. The residual condition was therefore characterized by visual inspection of crack propagation, delamination, and anchorage/connection damage.

The externally reinforced glulam timber beam specimen was composed of three main components: a metal fixture (refer to Fig. 2 (b)), steel supports (refer to Fig. 2 (c)), and the glulam beam itself. For the B-series beams, the external reinforcement consisted of 12-mm steel bars with a strength grade of Q345, yield strength of 345MPa, and ultimate strength of 630 MPa. The bars were arranged below the beam and anchored by the end steel fixtures. Before formal loading, a pre-tightening force of 5 kN was introduced into each steel bar by tightening the end anchorage system and was checked using torque-wrench calibration. This relatively low pre-tightening level was intentionally selected to avoid excessive local embedment of the end bolts into the timber and premature crushing around the anchorage region. Therefore, the B-series reinforcement should be interpreted as an externally anchored steel-reinforcement scheme with limited pre-tightening, rather than as a fully developed prestressed glulam system. The fully assembled specimen, incorporating all these elements, is illustrated in Fig. 2 (a). The beam-bottom steel plate reinforcement test specimen is designed to achieve full and intimate contact between the steel plate and the glulam beam. This is accomplished by driving self-tapping screws into the bottom surface of the glulam beam. The detailed dimensions of this reinforcement scheme are shown in Figs. 2 (d) and (e). The number and spacing of self-tapping screws were selected as a preliminary repair configuration by considering the beam size, steel-plate dimensions, constructability, minimum edge/end distances, and the need to distribute the clamping force along the damaged tension zone. An 80 mm spacing was adopted to provide a relatively uniform connection along the steel plate while reducing the risk of splitting caused by an excessively dense screw arrangement. However, this layout was not intended to represent an optimized screw configuration. The test results indicate that screw shear and local connection failure governed the later-stage response; therefore, the spacing, diameter, penetration depth, and arrangement of self-tapping screws should be further optimized in future parametric studies.

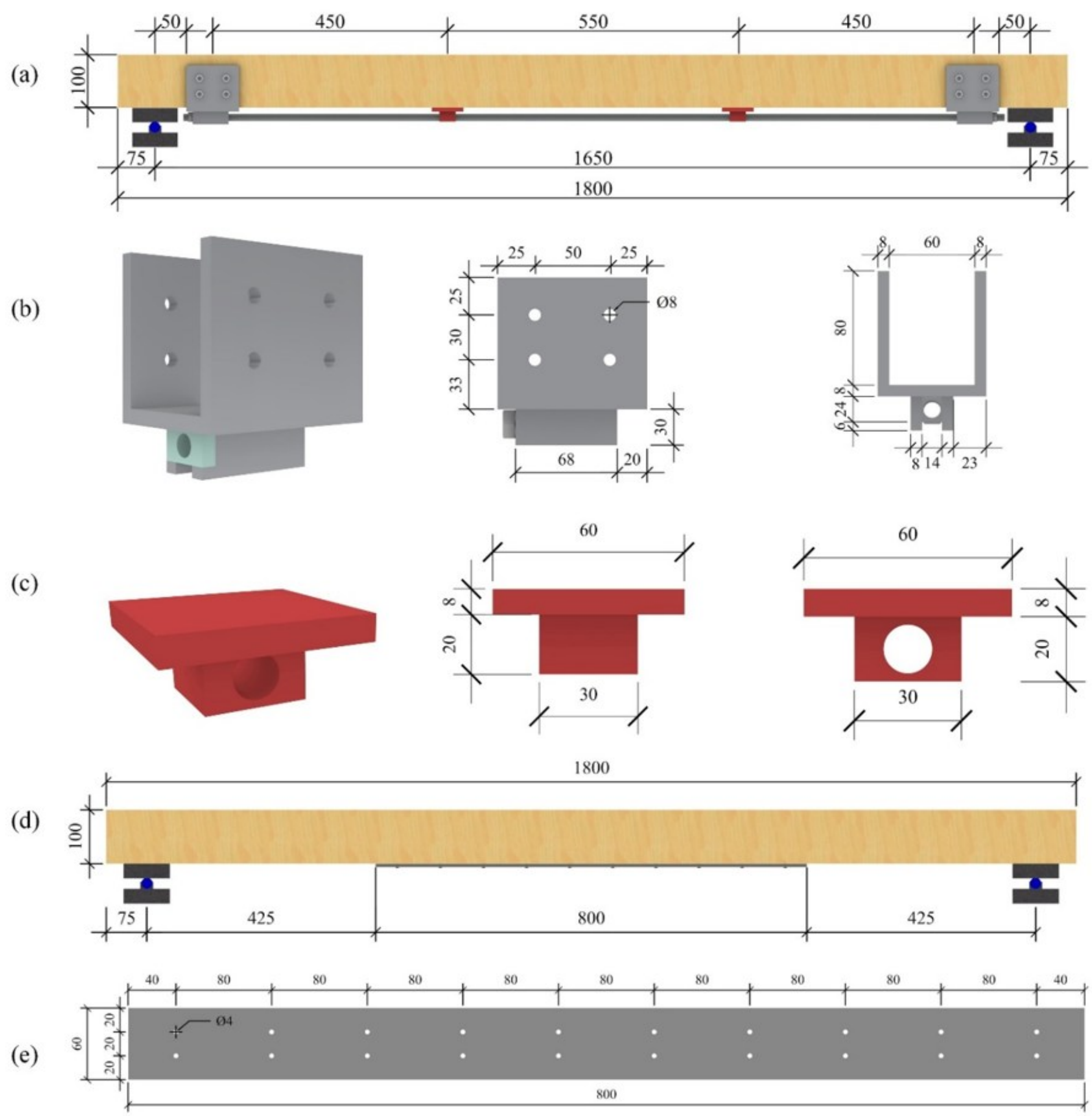

Fig. 2. Geometric dimensions and reinforcement configuration of test beams: (a) schematic of the overall assembly of externally reinforced glulam beam; (b) dimension diagram of fixture; (c) dimension drawing of support device; (d) overall dimensions drawing for steel plate reinforced glulam beam; and (e) dimension drawing of steel plate

The main machining procedures for reinforced glulam beam specimens consist of several critical steps. Initially, precise positioning and layout are conducted to establish the exact locations where machining will take place. Following this, a sequence of operations is performed, which includes drilling the components, grinding the surfaces, and cleaning the drilled holes. The final step involves the attachment of strain gauges to the prepared specimens. Detailed descriptions of the specific operational methods for these processes are illustrated in Fig. 3.

(a)

(b)

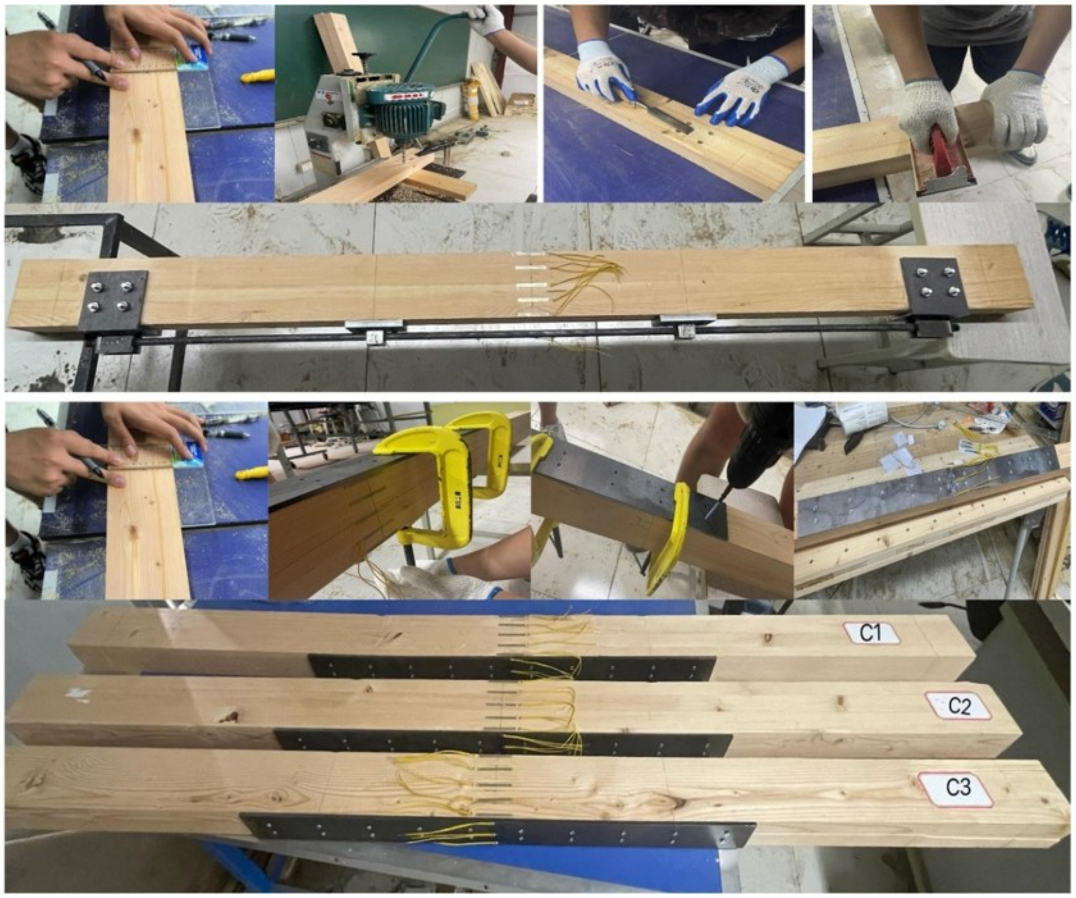

Fig. 3. Reinforcement process: (a) B series and (b) C series

Loading Protocol and Measurement Arrangement

The four-point bending test was performed utilizing an electro-hydraulic servo-controlled loading system. The setup included a reaction frame, load and displacement sensors, a force-distribution beam, and rigid loading pads. A hydraulic actuator with a maximum capacity of 200 kN was employed to apply load in stages. Vertical force from the actuator was transferred through the force-distribution beam to produce two symmetric point loads on the specimen. Prior to formal testing, a preloading cycle between 2 and 5 kN was applied and then fully removed to minimize system compliance and seating errors, ensuring that the initial conditions approximated actual service loading. During the linear-elastic response phase of the material, the load was increased in increments of 2 kN per stage. After the specimen behaviour deviated from linear elasticity, the increment was reduced to 1 kN per stage until ultimate failure was reached. Each load stage was held constant for 120 s to allow for stabilization, during which all monitoring data were recorded synchronously. The test monitored mid-span deflection, strain distribution across the beam section at mid-span, and strain in the reinforcing steel plate. Instrumentation consisted of five linear variable displacement transducers (LVDTs), designated as W1 through W5, installed at both support locations, under each loading point, and at the mid-span. For the unreinforced control glulam beams and externally reinforced glulam beams, five electrical resistance strain gauges (S1 to S5) were mounted at equal vertical intervals along the side face at mid-span to capture the strain profile over the beam depth. For the steel-plate-reinforced glulam beam, an additional strain gauge (S6) was attached to the tension face of the steel plate at the mid-span section. The detailed loading protocol and instrumentation layout are illustrated in Fig. 4.

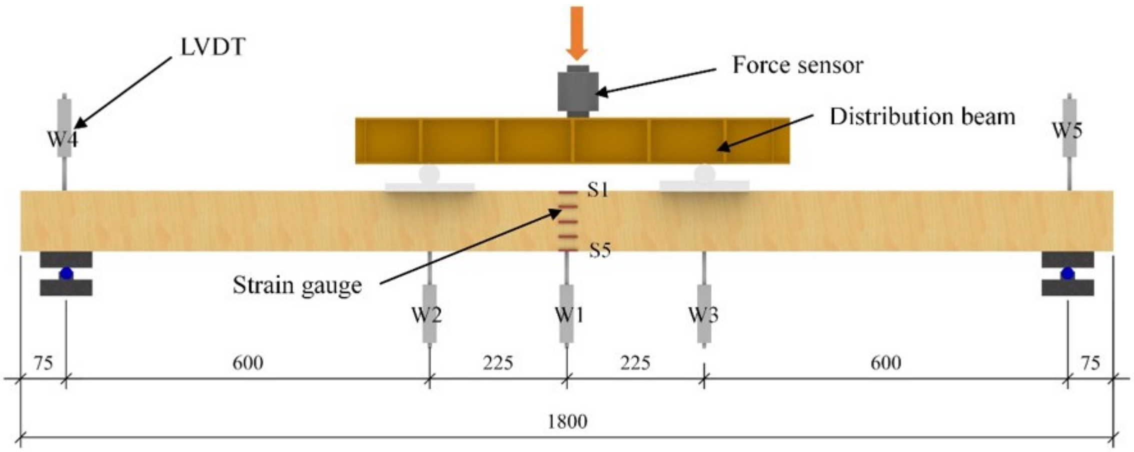

Fig. 4. Schematic diagram showing the layout of the loading equipment and measurement points

RESULTS AND DISCUSSION

Typical Failure Modes

Unreinforced glulam beams

As illustrated in Fig. 5, the unreinforced control glulam beam exhibited the typical mechanical behaviour of glulam beams when subjected to loading. The primary failure mode observed in this type of beam consists of fiber-tearing failure at the bottom of the beam and shear failure within the wood material. Additionally, the presence of knots introduces certain variations and shifts in the failure behaviour of the beam. As illustrated by specimen A1, the relationship between the applied load and beam displacement during the initial phase of loading was predominantly linear.

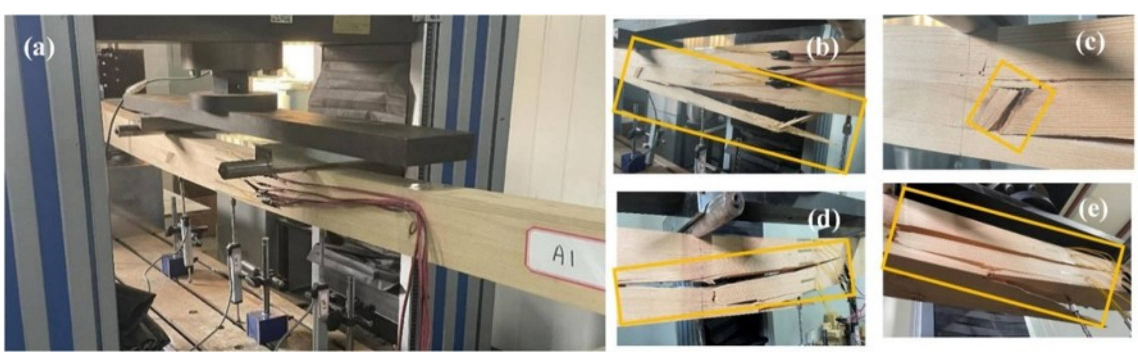

Fig. 5. Typical failure of unreinforced glulam beams

Upon reaching a load of approximately 10 kN, the beam began to emit faint acoustic signals. As the load was increased to approximately 16.7 kN, the beam began to emit continuous cracking sounds, and initial cracks aligned with the wood grain became visible (see Fig. 5 (b)). As the loading continued, distinctive crackling sounds indicative of tearing were audible, and cracks located proximally to the knots began to propagate more noticeably (see Fig. 5 (c)). When the applied load reached 23.79 kN, the beam abruptly emitted a loud cracking noise, followed by severe splitting along the bottom surface (Fig. 5 (d)). This was immediately followed by a brittle tensile failure of the beam (Fig. 5 (e)), which marked the conclusion of the test.

Externally reinforced glulam beams

For externally reinforced glulam beams, the incorporation of prestressed steel bars at the bottom altered the typical failure mechanism. However, as the prestressing elements were confined to the beam ends, their synergistic interaction and reinforcing efficiency did not fully exhibit the expected performance. Consider specimen B1 as a representative case: In the early stages of loading, the load-displacement response of the timber beam demonstrated a predominantly linear behaviour.

At a load of approximately 11 kN, minor flexural deformation was observed, accompanied by faint acoustic emissions. Upon reaching about 15 kN, continuous splitting noises emerged, and distinct cracks became visible along the grain direction. With further loading, localized wrinkling developed near the point of load application (refer to Fig. 6 (b) and (c)), concurrent with persistent crackling sounds indicative of wood fiber separation. Cracks progressively widened at the beam's knot locations, bolt holes within the end metal connectors exhibited slippage, and noticeable bending deformation occurred in the tensile region beneath the beam.

Notably, the reinforcing bars had not yet transitioned into an effective stress state at this phase. When the load attained 23.5 kN, the wooden beam experienced sudden failure accompanied by a pronounced cracking sound. Extensive longitudinal cracks propagated along the beam bottom (Fig. 6(d)). At the end anchorage region, local indentation and relative movement between the external steel bar/fixture system and the timber were observed after peak loading, indicating that the external reinforcement did not remain fully engaged with the timber member.

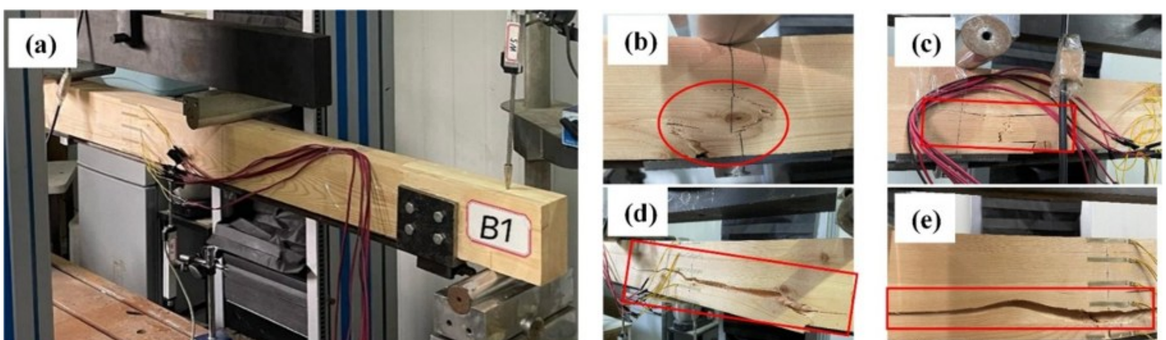

Fig. 6. Typical failure of externally reinforced glulam beams

Steel plate-reinforced glulam beams

The failure mode of the steel-plate reinforced beams was unique and different from other specimens. This was because they were made from damaged glulam beams as the base material and were strengthened with steel plates using self-tapping screws. The beams mainly failed due to interlaminar tearing within the glulam beams. Using Specimen C1 as an example, during the initial loading phase, the load-displacement curve of the timber beam showed a predominantly linear relationship.

As the applied load increased to approximately 10 kN, the glulam component and the steel plate came into full contact and began to share the stress equally. At this stage, faint cracking sounds could be heard coming from the wooden beam. When the load reached around 15 kN, the glulam beam continued to emit cracking noises, accompanied by tear failure propagating along the grain direction between adjacent timber layers (as shown in Fig. 7(b)). At the same time, pre-existing knots in the wood cracked again under the increasing load.

With further loading, more pronounced crackling sounds indicative of progressive tearing became audible. The steel plates at both ends of the beam gradually lifted and separated from the timber, and the self-tapping screws connecting the two materials sheared off and detached (see Fig. 7 (c)). Ultimately, when the load peaked at 16.9 kN, a continuous crack developed along the grain of the glulam beam, leading to tensile failure at the knot locations (as illustrated in Fig. 7 (d)), marking the end of the test.

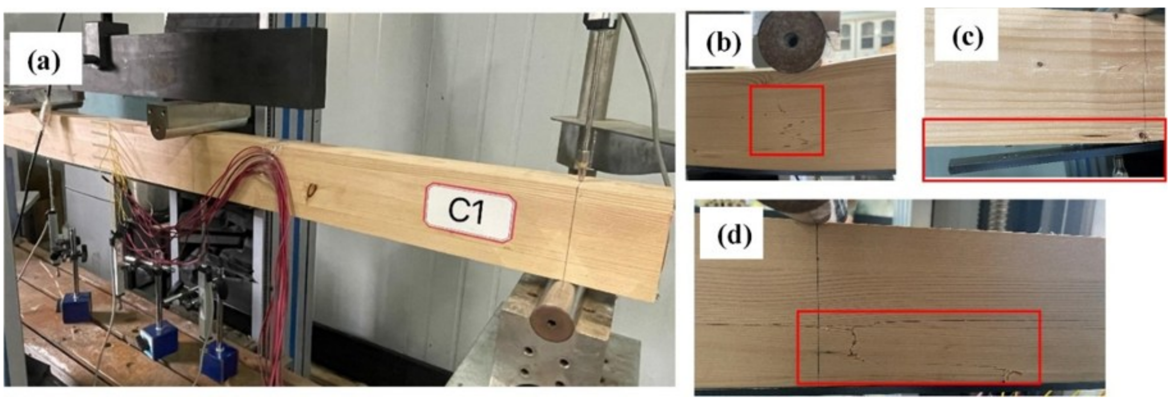

Fig. 7. Typical failure of steel plate-reinforced glulam beams

Load-midspan Deflection Curves

Figure 8 presents the load-deflection curves for three sets of test specimens. As observed in the figure, during the initial loading stage, all glulam beams exhibited comparable stiffness, with the load and deflection maintaining an approximately linear relationship. This linear trend reflects the material primarily functioning within its elastic domain. With further loading, the beams progressively enter an elastic-plastic state, where the slope of the load-deflection curve diminishes consistently, marking the departure from linearity. Simultaneously, the deflection rate accelerated considerably.

A detailed inspection of Fig. 8 (b) reveals that the load-deflection curves for externally reinforced glulam beams aligned closely with those of the unreinforced control beams in the early loading phase. This close overlap implies that the external reinforcement had a negligible effect on improving either the ultimate load capacity or the overall deformation characteristics under the given test conditions. In contrast, Fig. 8 (c) demonstrates that glulam beams reinforced at the bottom exhibited markedly different mechanical behaviour.

While their ultimate load-bearing capacity reached only about 75% of that of the benchmark (unreinforced or conventionally reinforced) beams, these bottom-reinforced specimens showed a substantial gain in deformation capacity.

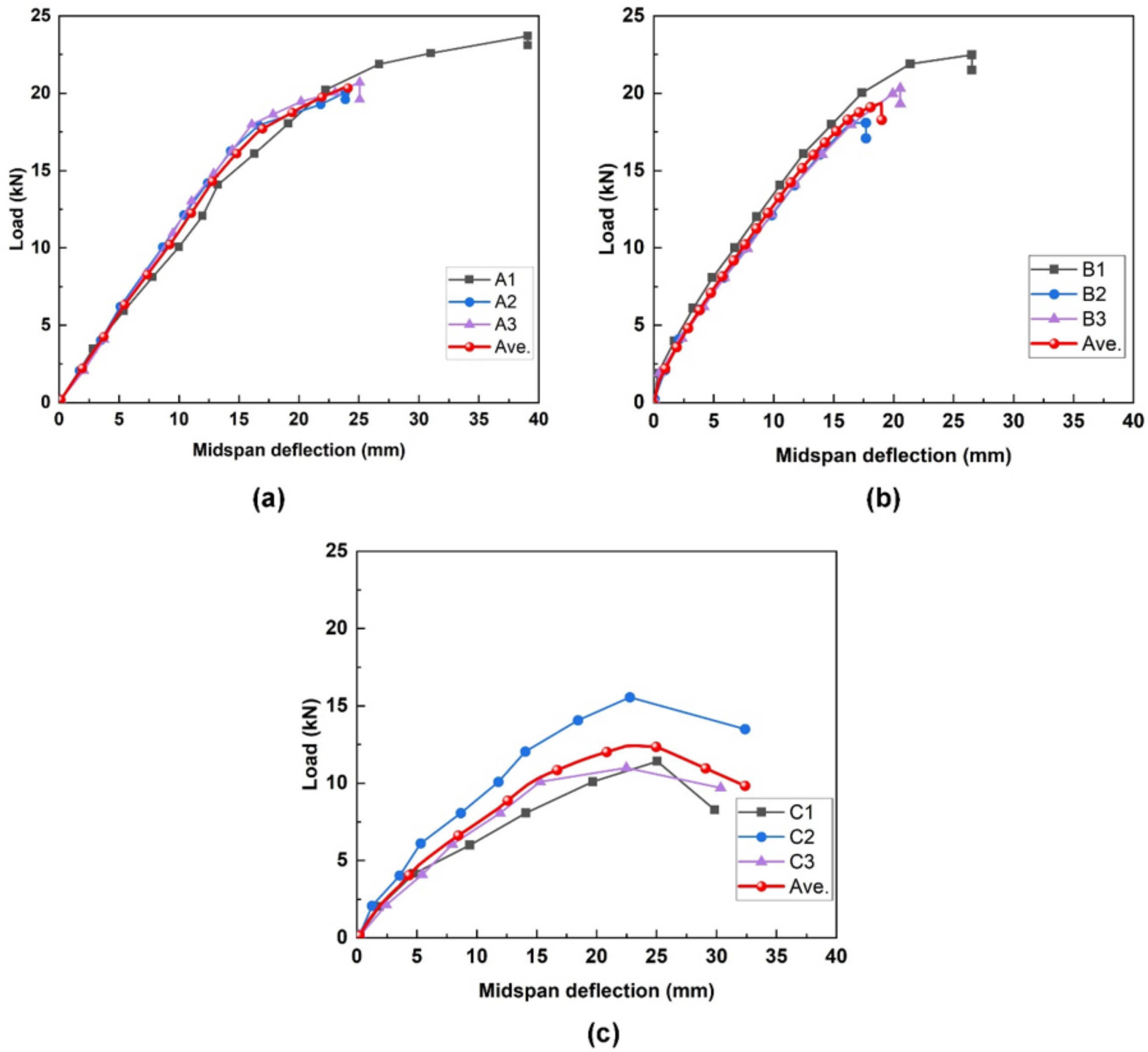

Fig. 8. Experimental load- midspan deflection curves: (a) unreinforced glulam beams; (b) externally reinforced glulam beams; and (c) steel plate-reinforced glulam beams

Load-strain Curves

Figure 9 presents the load-strain curves for three configurations of glulam beams subjected to varying load levels. A comparative assessment demonstrates that the employed reinforcement techniques exerted a substantial influence on the structural performance of these beams. As illustrated in Figs. 9 (a) to (c), the unreinforced control beam displayed characteristic mechanical behaviour typical of timber materials under loading. During the initial loading stage, beam strain exhibited a predominantly linear and symmetrical distribution, with the upper region in compression and the lower region in tension. As the applied load increased progressively, the entire beam operated within its elastic deformation range. However, upon approaching and reaching the ultimate load-bearing capacity, the strain response deviated from linearity, undergoing an abrupt transition that culminated in instantaneous brittle tensile failure at the beam's bottom fiber. This failure mode, characterized by its sudden nature and lack of pronounced warning, underscores the inherent limitations of unreinforced timber beams in terms of both load capacity and ductility.

As illustrated in Figs. 9 (d) to (f), the load-strain curve for the beam reinforced with external prestressed steel bars demonstrated a noticeable degree of nonlinearity. In comparison to the control specimen, the slope of the curve within the tensile zone at the bottom of the beam was increased, indicating that the external reinforcement provides a measurable enhancement to the tensile performance of beams. However, it is evident from the strain data recorded by gauge No. 6 on the bottom flange that, with further load escalation, the strain increment no longer maintained a consistent linear relationship with load. This finding indicates that the combined effect of the externally applied prestressed bars and the timber substrate was suboptimal, leading to inadequate stress transfer and substandard compatibility between the two materials. Consequently, while this external reinforcement method offered a moderate improvement in stiffness, its overall effectiveness was constrained, failing to fully utilise the potential of the reinforcing material.

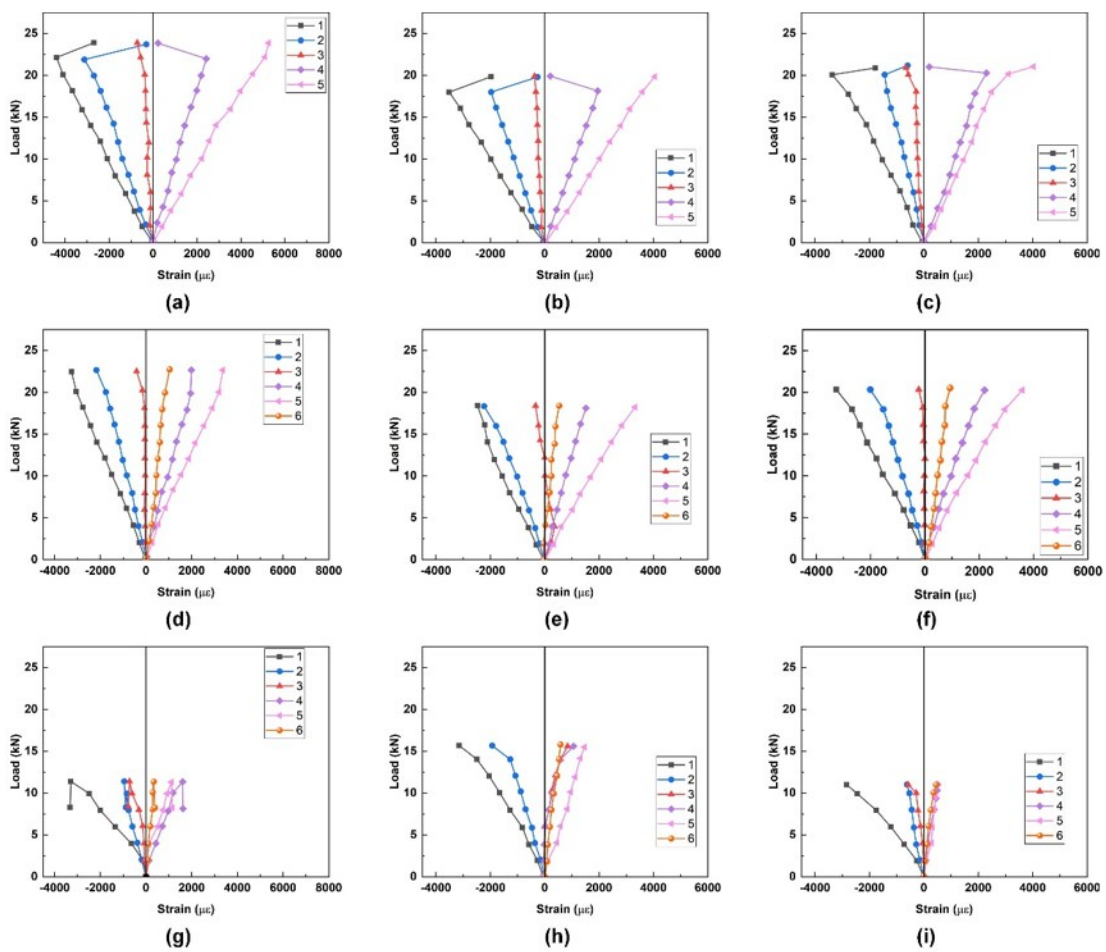

Fig. 9. Load–strain curves: (a) to (c) unreinforced glulam beams; (d) to (f) externally reinforced glulam beams; and (g) to (i) steel plate-reinforced glulam beams

For the glulam beams reinforced with steel plates, the load-strain behaviour diverged notably from that of the preceding two specimens, partly due to pre-existing damage within the original timber. As shown in Figs. 9 (g) to (i), during initial loading, the strain in the steel-plated beam also increased in an essentially linear manner, indicative of elastic response. However, once the load surpassed a critical threshold, the deformation behaviour deviated from linearity, producing a distinct inflection point on the strain-load curve. Specifically, in the early loading phase, the strain measured by gauge No. 6 in the tensile zone beneath the beam continued to rise linearly. Yet, when the load reached approximately 50% of the ultimate capacity, the reading from gauge No. 6 began to register lower values than those from gauge No. 5. This shift signaled the onset of effective interaction between the timber and the steel plate, enabling cooperative load-bearing. However, as loading progressed into advanced stages, the strain value from gauge No. 6 stabilized or exhibited negligible change. This observation implies that the screw fasteners connecting the steel plate to the timber may have experienced shear failure or loosening, leading to debonding at the interface. As a result, the steel plate could no longer contribute effectively to load resistance. Concurrently, extensive through-thickness cracks developed within the internal laminations of the timber beam, ultimately precipitating failure *via* tensile rupture. This failure mechanism highlights certain deficiencies in the steel plate reinforcement approach, particularly concerning connection reliability and long-term performance stability, with the screw attachment points emerging as vulnerable weak links.

Bearing Capacity, Stiffness, and Ductility

Table 2 presents the primary test results for the test beams, including the mean values for each specimen group. Flexural stiffness is a vital metric for assessing the resistance to deformation in structures or components. In accordance with the stipulations set out in the "Code for Design of Timber Structures" (GB 50005 2017), within the elastic range, the load-midspan deflection curve maintains a linear relationship with a constant slope, thereby ensuring a linear proportionality between the two variables. Consequently, the stiffness of beam remained constant throughout this phase. Prior to the mid-span deflection reaching $l_0/180$ (Wan *et al.* 2025), stiffness is calculated using Eq. 1. The ductility coefficient is determined by Eq. 2, where the yield displacement Δf is established using the "furthest point method" proposed by Feng *et al.* (2017).

Table 2. Summary of Experimental Values

Specimen Code	P_{max} (kN)		Δ_{max} (mm)		EI (10^{11} N.mm^2)		μ_f		Failure Mode
	Exp	Mean Value	Exp	Mean Value	Exp	Mean Value	Exp	Mean Value	
A1	23.8	21.6	39.6	29.47	0.5	0.6	1.6	1.4	A
A2	19.8		23.8		0.7		1.3		A
A3	21.0		25.0		0.7		1.4		A
B1	23.5	20.7	26.2	21.47	0.8	0.8	1.3	1.0	A
B2	18.2		17.6		0.9		1.0		B
B3	20.3		20.6		0.8		0.9		B
C1	15.6	16.4	25.0	23.33	0.5	0.6	1.2	1.5	B
C2	16.9		22.5		0.6		1.6		C
C3	16.7		22.5		0.6		1.8		B

Notes: P_{max} = Ultimate load; Δ_{max} = Mid-span deflection; EI = Flexural Stiffness; u_f = Ductility coefficient; Failure mode: A = tensile failure at the beam bottom; B = delamination between glulam laminae; C = separation/delamination between the steel plate and the glulam beam.

$$EI = \frac{Pa(3l^2 - 4a^2)}{48f} \tag{1}$$

$$\mu_f = \frac{\Delta_{0.8P_{\max}}}{\Delta_f} \tag{2}$$

In Eqs. 1 and 2, P denotes the applied load, a represents the distance from the loading point to the support, l signifies the clear span between supports, and f indicates the mid-span deflection.

As demonstrated in Table 2, when contrasted with the unreinforced control glulam beams, the externally reinforced glulam beams demonstrated not only a decline in stiffness but also a reduction in both load-bearing capacity and ductility. These findings suggest that the reinforcement technique employed did not achieve the intended strengthening objectives. The application of prestress confined exclusively to the beam ends was found to be ineffective in ensuring the efficient transfer of prestress forces across the entire member. In essence, this method of prestressing reinforcement merely transferred the applied loads from the bottom tension reinforcement to the upper bolts, without establishing a fully integrated and functionally effective prestressing system along the length of the beam. Consequently, the reinforcement primarily provided localised support and protection at the base of the beam, resulting in a shift in the failure mode from tensile failure in the bottom tension zone of the timber to delamination within the laminated layers. The following factors have been identified as the primary contributors: (1) The limited pre-tightening level and the end-anchorage configuration did not allow efficient prestress transfer along the beam; (2) Poor interaction between the timber and the reinforcement material led to premature failure of the timber itself, while the reinforcement carried minimal load; (3) Furthermore, there was occurrence of slippage at the metal end connections. For beams that were reinforced with bottom steel plates, this reinforcement strategy was able to restore approximately 76% of the flexural load-bearing capacity of beams after complete failure, when compared to that of ordinary glulam beams. However, there is still room for improvement, for instance through the use of screws with higher tensile strength and by optimising the spacing and arrangement configuration of the screws to enhance overall load transfer and structural performance.

It should be noted that only three specimens were tested in each group. This sample size is common in exploratory full-scale timber tests but is insufficient for robust statistical inference. Therefore, the reported differences among the A-, B-, and C-series beams should be interpreted as experimental trends rather than statistically generalized design values. The coefficients of variation of ultimate load were approximately 9.5% for the A-series, 12.9% for the B-series, and 4.3% for the C-series based on the values in Table 2, indicating acceptable repeatability for the main load-capacity trend within this limited dataset. Nevertheless, additional specimens, more timber batches, and probabilistic analysis are required before the proposed conclusions can be generalized for design practice.

FE Modeling-Constitutive Model of the Materials

All numerical simulations were performed using Abaqus/CAE 2020 with the Abaqus/Standard implicit solver. Three-dimensional solid models were established for the glulam beams, steel plates, bolts, steel bars, self-tapping screws, loading blocks, and supports. Nonlinear material behaviour, surface-to-surface contact, and displacement-controlled quasi-static loading were included in the simulations.

Glulam

This section employs the Hoffman yield criterion (Hoffman 1967) in conjunction with the anisotropic material modelling framework pioneered by Sandhaas (2012) to comprehensively characterise the elastic-plastic and damage behaviour of glulam. This methodology captures the mechanical response of glulam across its principal material orientations (longitudinal, radial, and tangential) by modelling it as a homogeneous, continuous, and anisotropic elastoplastic continuum (Eslami *et al.* 2021). In the simulations, damage initiation was evaluated using the Hoffman interaction criterion rather than by comparing the longitudinal tensile stress alone with the clear-specimen tensile strength. The first critical regions were located at the lower tensile zone and near stress-concentration zones, where longitudinal tension was combined with transverse tensile stress and longitudinal-radial/longitudinal-tangential shear components. Therefore, the apparent nominal bending stress at peak load can be lower than the longitudinal clear-specimen tensile strength while the interaction criterion is still reached locally. In lieu of an explicit representation of the layered composition and finger-jointed connections inherent within the timber structure, the model abstracts glulam as a unified anisotropic material.

For material assignment in the FE model, all three-dimensional elements belonging to the same component were assigned the same material definition. The glulam elements in the A and B series were assigned the homogeneous anisotropic elastoplastic properties listed in Tables 3 and 4. For the C series, which used pre-damaged glulam beams, the elastic moduli and strength parameters of the glulam elements were reduced by 25% to represent the residual material condition after prior failure. The 25% degradation factor used for the C-series model was a simplified calibration parameter introduced to represent the damaged condition of reused glulam beams. It was not independently obtained from separate residual material tests. Therefore, the good agreement between the C-series FE curves and the experimental curves should be interpreted as calibrated reproduction of the observed response and failure mechanism, not as independent prediction. In contrast, the A- and B-series simulations were based directly on the measured material parameters and provide the primary validation of the modelling strategy. Future studies should determine residual material properties through independent post-damage mechanical testing or nondestructive evaluation before FE prediction of repaired timber members.

Table 3. Elastic Mechanical Parameters of Glulam

Modulus of Elasticity (MPa)			Poisson's Ratio			Shear Modulus (MPa)		
E_{11}	E_{22}	E_{33}	υ_{12}	υ_{13}	υ_{23}	G_{12}	G_{13}	G_{23}
11380	1138	640	0.37	0.43	0.63	1268	1014	304

Notes: *L* denotes the longitudinal direction, *R* is the radial direction, *T* is the tangential direction, E_i is the modulus of elasticity in the i-direction, G_{ij} is the shear modulus of the i-j shear plane, and v_{ij} denotes Poisson's ratio

Table 4. Material Properties of GLT in Plastic Stage

Compressive Yield Stress (MPa)			Tensile Strength (MPa)			Shear Yield Stress (MPa)		
L	R	T	L	R	T	L	R	T
36.0	5.25	5.05	85.5	5.15	5.04	8.4	7.5	7.5

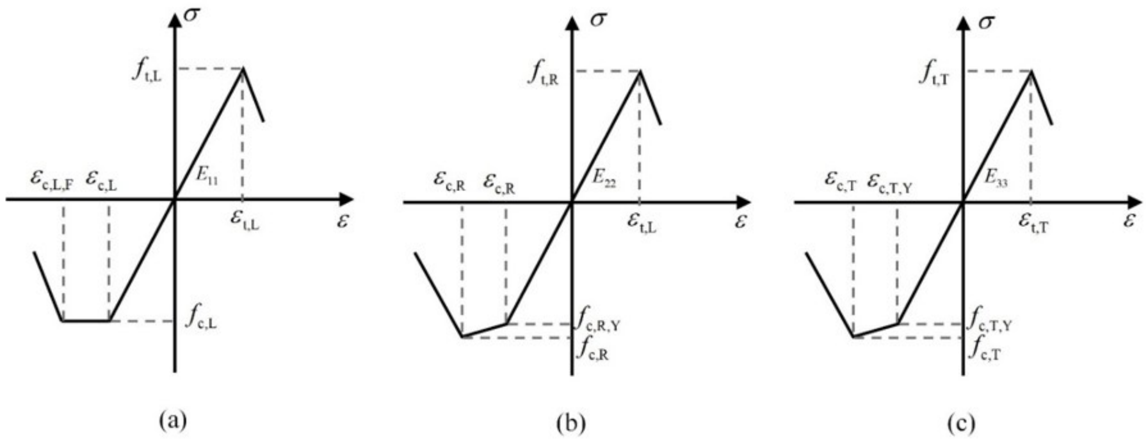

Fig. 10. Stress-strain relationship of GLT in various directions: (a) Longitudinal direction; (b) Radial direction; and (c) Tangential direction

Steel component

A bilinear elastoplastic constitutive model was employed for the numerical simulation and analysis of steel plates, bolts, and self-tapping screws. As detailed in earlier, the material parameters for these components were consistently defined: the elastic modulus was uniformly set to 2.1×10^5 MPa, and Poisson's ratio was uniformly set to 0.3. Regarding the specific mechanical properties of each component, the yield strength of the steel plate was 463 MPa, the yield strength of the bolt was 635 MPa, and the yield strength of the self-tapping screw was 489 MPa.

Mesh Properties

The standard finite element (FE) model used in this study was built with an 8-node linear brick solid element (C3D8R type), which is a type of three-dimensional solid element that employs the reduced integration method for numerical computation. Furthermore, to systematically assess the influence of mesh density on the accuracy and reliability of the simulation results, three different mesh partitioning strategies were implemented: a fine mesh with an element size of 10 mm, a medium mesh with an element size of 20 mm, and a coarse mesh with an element size of 30 mm. Figure 11 illustrates the results of the sensitivity analysis conducted on various mesh sizes within the control group of glulam beams. Using the control group beam as a representative case, it can be observed that the ultimate load-carrying capacity obtained with the fine mesh was slightly lower compared to those derived from the medium and coarse meshes. This discrepancy arises due to the strong correlation between mesh size and the damage iteration process. Specifically, excessively large mesh sizes impair the accurate detection of damage initiation within individual mesh elements, which in turn limits the precise representation of the material's constitutive behaviour. Nevertheless, when examining the overall trends depicted by the three curves, their general patterns show minimal variation. Taking into account both computational efficiency and the accuracy of the predictions, it is deemed appropriate to utilize the fine mesh for all subsequent numerical analyses. Additionally, Fig. 12 provides detailed illustrations of the mesh configurations applied to the various components of the specimens. It is imperative to acknowledge that this study adopted an integrated modelling methodology for the three types of fasteners: self-tapping screws, bolts, and reinforcing bars. The self-tapping screw model does not incorporate detailed thread geometry, whereas the bolt model includes the nut as an integral part of the assembly. It is important to note that these modelling simplifications have been validated in prior research (Bedon and Fragiacomo 2019; Yang *et al.* 2025; Li *et al.* 2026), with their feasibility and accuracy being thoroughly established.

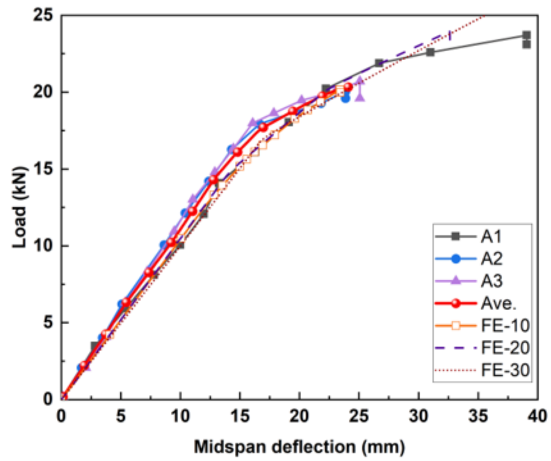

Fig. 11. Load-displacement from numerical study with different mesh sizes

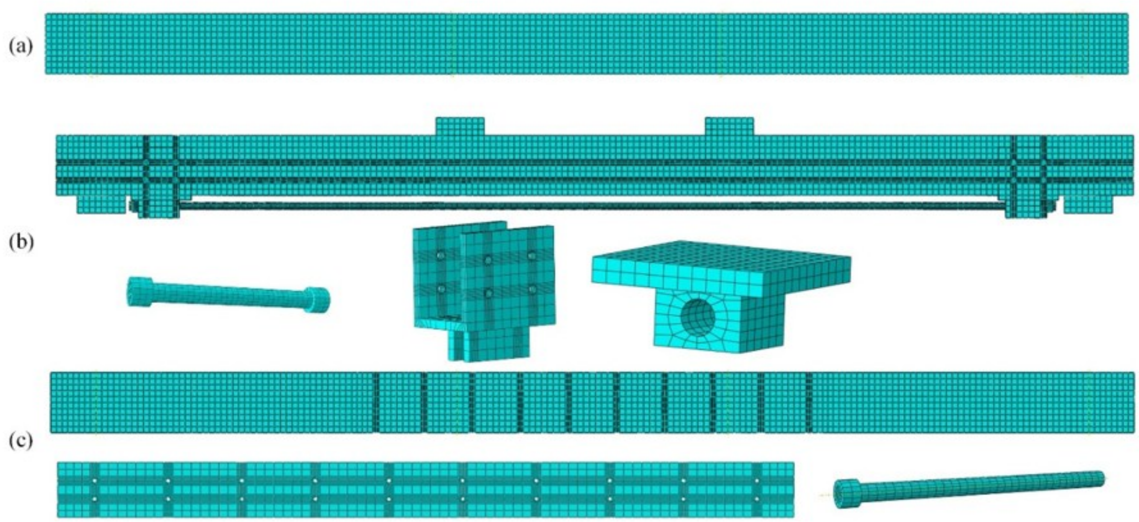

Fig. 12. Mesh division for different components: (a) unreinforced glulam beams; (b) externally reinforced glulam beams; and (c) steel plate-reinforced glulam beams

Contact, Loads, and Boundary Conditions

The contact interactions within this model encompassed several critical interfaces: the loading block to the glulam beam, the self-tapping screw to the glulam beam, the self-tapping screw to the steel plate, the steel plate to the glulam beam, the bolt to the glulam beam, and the bolt to the steel plate. All these interfaces are represented using surface-to-surface contact formulations. In the normal direction, each contact pair is configured with a rigid contact definition, while in the tangential direction, Coulomb friction models are applied to characterize the frictional behaviour. The specific friction coefficient values assigned to each contact pair are provided in Table 5.

Table 5. Contact Parameters

Component	Tangential Contact	Normal Contact	Master Surface	Slave Surface	Friction Coefficient
Block - Glulam Beam	Coulomb friction	Hard contact	Block	Glulam Beam	0.3
Steel Plate-Glulam Beam			Steel Plate	Glulam Beam	0.2
Self-tapping Screws - Glulam Beam			Self-tapping Screws	Glulam Beam	0.35
Self-tapping Screws Steel Plate			Self-tapping Screws	Steel Plate	0.1
Bolt - Glulam Beam			Bolt	Glulam Beam	0.2
Bolt-Steel Plate			Bolt	Steel Plate	0.15

In the FE simulation of glulam beams, boundary conditions were established using the supported reference point method. A fixed-hinge support was accurately modelled by fully constraining one reference point in all three translational degrees of freedom (U1, U2, and U3). Conversely, a sliding-hinge support, which restricts lateral displacement while permitting vertical movement, was simulated by constraining another reference point only in the U1 and U2 directions, leaving the U3 direction unconstrained. Load application was implemented through an independent loading point, which was kinematically coupled to both layers of the composite beam using coupled constraints. This coupling ensured efficient and uniform load transfer across the beam sections. The quasi-static loading process for the entire model was then executed by applying displacement control at this coupled loading point, thereby completing the simulation setup.

Validation of FE Model

Figure 13 provides a comparative analysis of the stress distribution and failure modes of glulam beams subjected to peak loading. As illustrated in Fig. 13 (a), the stress levels in the lower region of the glulam beam are substantially higher than those in the upper region, accompanied by clear signs of compressive wood damage localized near the loading point. The FE simulation results faithfully replicate this mechanical behaviour, thereby confirming that the proposed constitutive model is capable of accurately representing the mechanical response of glulam under complex loading scenarios. Moreover, the FE model suggests the failure modes observed in the externally stiffened glulam beam (Fig. 13 (b)). Specifically, it successfully captures key phenomena, such as the distinct compressive failure occurring in the pinned and slotted regions of the glulam adjacent to the bolted connection, as well as the separation of the steel clamp from the beam body once the peak load is reached. For the steel plate-reinforced glulam beams (Fig. 13 (c)), the simulation demonstrates acceptable agreement. The model effectively identifies and illustrates critical failure mechanisms, including interfacial debonding between the steel plate and the glulam beam, localized timber damage induced by the lateral resistance of self-tapping screws, and the specific failure patterns exhibited by the self-tapping screws themselves. In conclusion, the numerical model developed in this study offers a reproduced representation of the entire loading-to-failure process across various types of test beams.

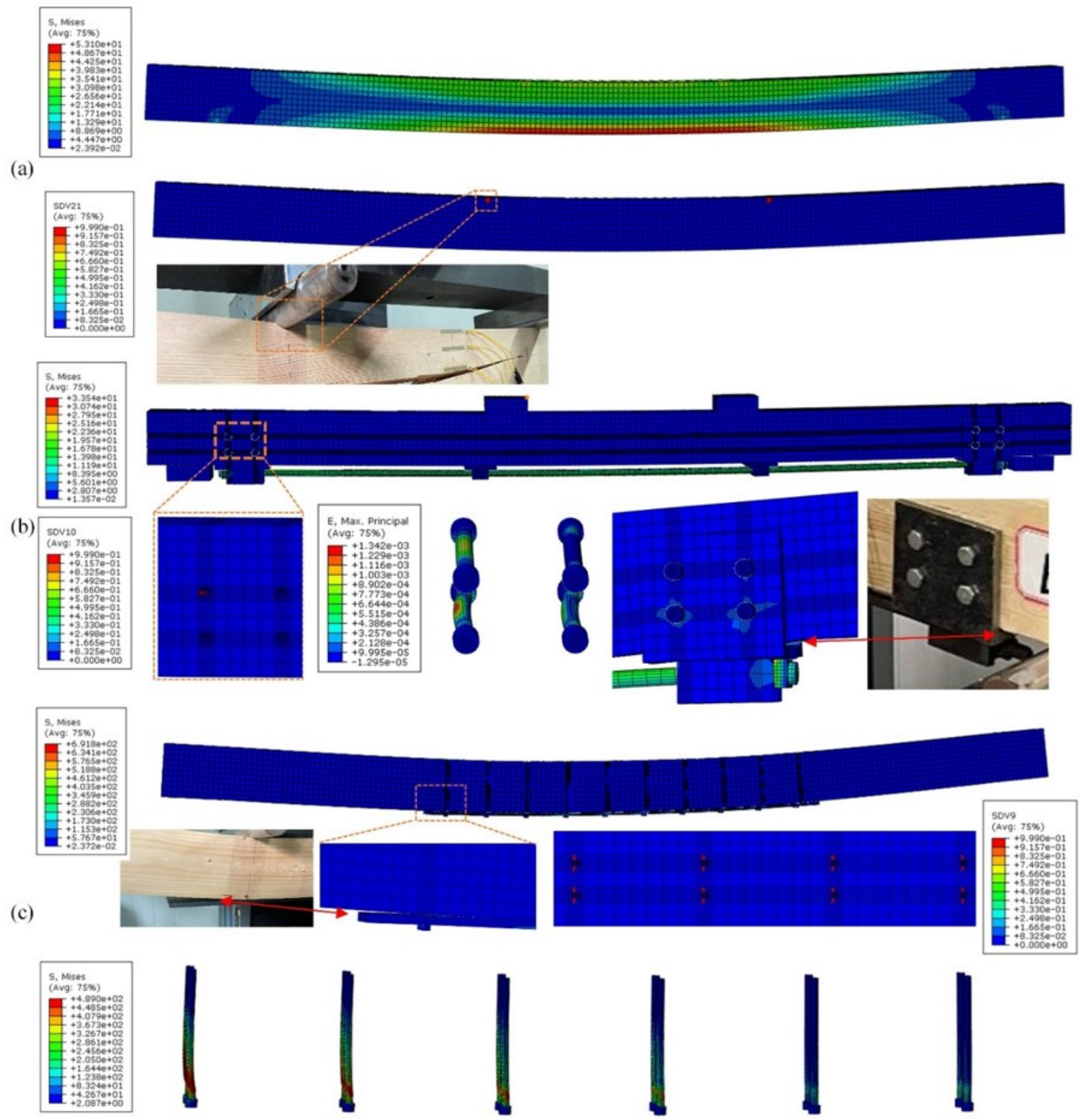

Fig. 13. Typical failure modes of glulam beams under peak loads: (a) unreinforced glulam beam; (b) externally reinforced glulam beam; and (c) steel plate-reinforced glulam beam

As illustrated in Fig. 14, the load-displacement relationship curves for the middle span were obtained through the combination of FE simulation and experimental testing. During the initial ascending phase of the curve, the simulated results closely corresponded to the experimental data, indicating that the established FE model accurately captured the mechanical behaviour of the composite beam during its elastic working stage. It is evident that only minor discrepancies existed in the prediction of initial stiffness and ultimate load-bearing capacity. Conversely, the numerical model also successfully reproduced the characteristic abrupt load capacity drop after peak load, caused by the failure of the glulam material. To further validate the accuracy of model, Fig. 15 compares the experimental load-strain curves of specimens A1, B1, and C1 with their corresponding FE simulation results. The strain development patterns obtained from FE simulations demonstrated a high degree of alignment with the trends observed in the tests, with only minor deviations recorded at a few localized measurement points. In summary, the numerical model established and employed in this study reliably reflected the overall mechanical behaviour of the test beams.

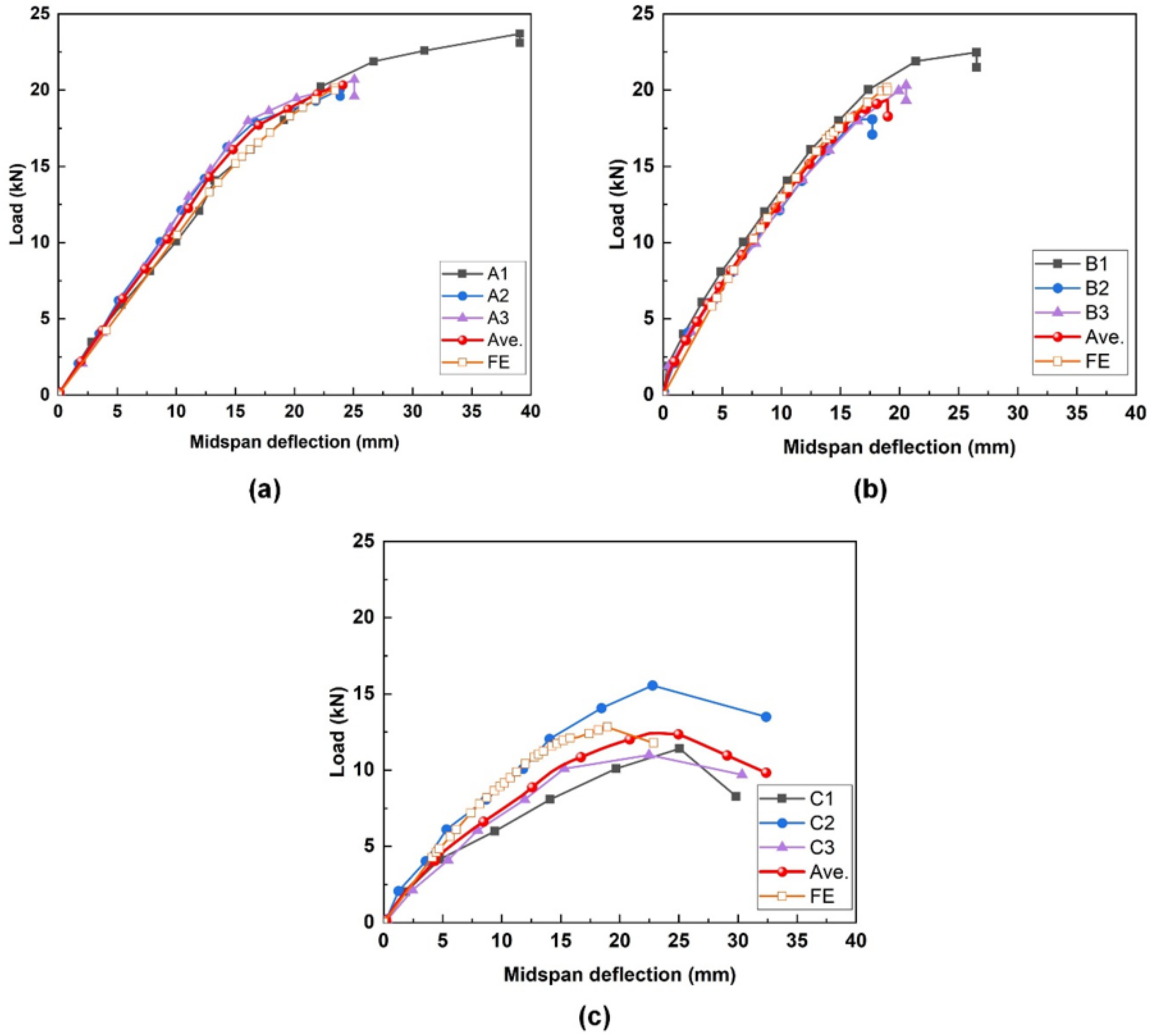

Fig. 14. Comparison of experimental and FE load-displacement curves: (a) unreinforced glulam beams; (b) externally reinforced glulam beams; and (c) steel plate-reinforced glulam beams

To further quantify the agreement between the FE and experimental results, statistical validation was performed based on the average load–midspan deflection curves, as summarized in Table 6. The FE load values were interpolated at the corresponding experimental displacement points within the common deflection range. The peak-load errors were within 5% for all three specimen groups, indicating that the FE model accurately predicted the load-bearing capacity. The NRMSE values were 3.47%, 2.29%, and 9.50% for groups A, B, and C, respectively, while the corresponding R^2 values were 0.987, 0.994, and 0.893. These results confirm that the numerical model provided a reliable representation of the global flexural response. The slightly larger deviation observed for the C-series beams was mainly related to the pre-existing damage in the glulam beams and the nonlinear contact and slip behaviour between the steel plate, self-tapping screws, and timber.

Table 6. Comparison of Experimental and FE Results

Specimen group	Peak load (kN)		Error (%)	Initial stiffness (kN/mm)		Error (%)	MAE (kN)	RMSE (kN)	NRMSE (%)	R^2
	EXP	FE		EXP	FE					
A	20.36	20.17	−0.96	1.13	1.04	−8.00	0.64	0.71	3.47	0.987
B	19.37	20.21	4.31	1.26	1.36	7.33	0.36	0.44	2.29	0.994
C	12.43	12.84	3.31	0.80	1.01	26.13	1.00	1.18	9.50	0.893

Notes: The FE load values were interpolated at the experimental displacement points within the common deflection range. The error was calculated as (FE − Exp.)/Exp. × 100%. The initial stiffness K0 was obtained by linear regression over the 10% to 40% range of the experimental peak load extracted from the mean load–deflection curve. MAE = mean absolute error; RMSE = root mean square error; NRMSE = RMSE normalized by the experimental peak load from the mean curve.

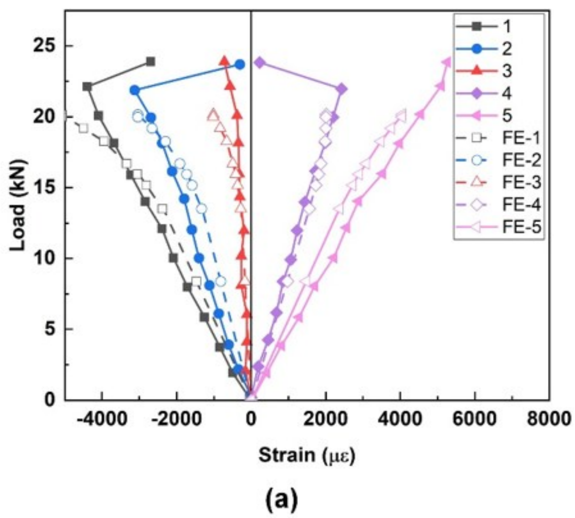

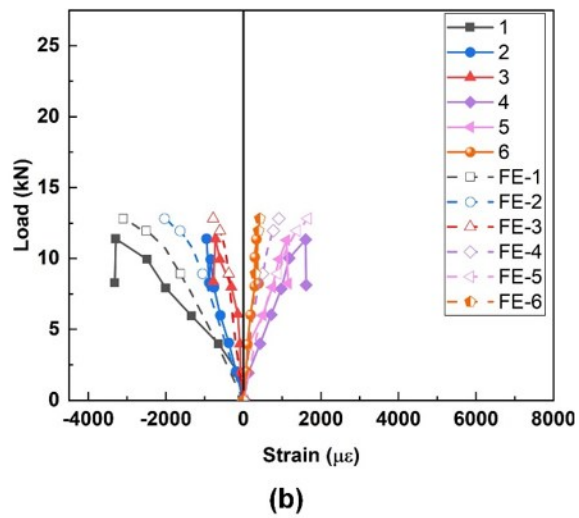

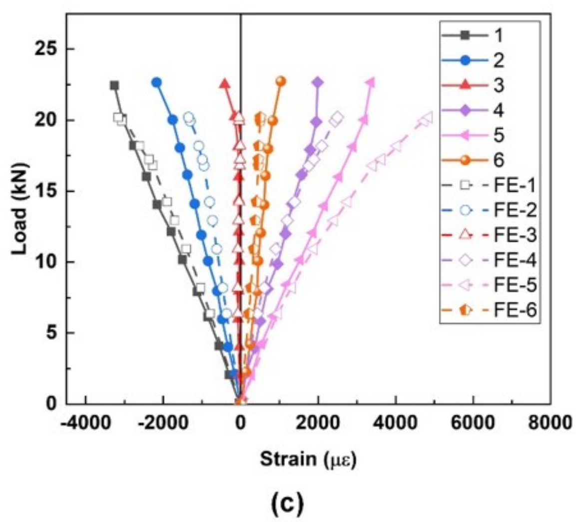

Fig. 15. Comparison of experimental and FE load–strain curves at corresponding strain-gauge locations: (a) A1; (b) B1; and (c) C1. FE1–FE5 correspond to the simulated strain responses at the positions of gauges S1–S5 on the glulam beam, and FE6 corresponds to the simulated strain at the steel-plate gauge position

CONCLUSIONS

This study experimentally and numerically investigated the flexural performance of glulam beams reinforced by two practical reinforcement schemes (external steel reinforcement and bottom steel plate reinforcement with self-tapping screws), with unreinforced glulam beams as the control group, aiming to address the brittle tensile failure of glulam beams in the tension zone and the underutilization of material performance, and to provide feasible reinforcement schemes for the retrofit of damaged glulam structures. A series of full-scale four-point bending tests were conducted to analyze the failure modes, load-deflection relationships, load-strain characteristics, as well as the bearing capacity, stiffness and ductility of the beams, and a three-dimensional FE model was established and validated to reveal the mechanical response mechanism of reinforced glulam beams. The key findings and conclusions of this research are summarized as follows:

1. The unreinforced glulam beams exhibited typical brittle tensile failure at the beam bottom accompanied by shear failure, with sudden failure without obvious warning and a mean ultimate load of 21.6 kN. The externally reinforced glulam beams with prestressed steel bars at the ends still presented brittle failure characteristics similar to the control group, with a mean ultimate load of 20.7 kN and reduced stiffness and ductility. The primary causes included limited pre-tightening and inefficient prestress transfer, poor interfacial interaction between steel and timber, and slippage at metal end connections, leading to ineffective stress transfer and underutilization of reinforcement materials. The steel plate-reinforced beams showed a change in failure process from sudden bottom tensile rupture to progressive interlaminar tearing, screw shear, and local steel-plate separation. However, the mean ductility coefficient increased only slightly from 1.4 for the control beams to 1.5 for the C-series beams. Therefore, the improvement should be described as a limited increase in deformation capacity and a more progressive damage process, rather than a clear transformation to a ductile failure mode.

2. The load-strain analysis revealed distinct mechanical responses of the three types of beams: the unreinforced beams showed linear and symmetrical strain distribution in the elastic stage with abrupt brittle failure at ultimate load; the externally reinforced beams exhibited increased slope of the tensile zone strain curve but nonlinear strain development at high loads due to poor steel-timber compatibility; the steel plate-reinforced beams presented an inflection point in the load-strain curve at 50% of the ultimate load, where the steel plate and timber initially achieved cooperative load-bearing, while subsequent screw failure and interfacial debonding led to the loss of the steel plate's reinforcement effect. The load-deflection curves of all beams showed linear elasticity in the initial stage, and the deviation from linearity marked the entry into the elastoplastic stage; the external steel reinforcement had negligible improvement on the deformation characteristics of glulam beams. The bottom steel plate reinforcement changed the damage-development process of the retrofitted beams and allowed the damaged beams to sustain load after initial crack development, although the improvement in ductility was limited and the ultimate capacity did not exceed that of the intact control beams.

3. The finite element (FE) model reproduced the main load-displacement response, strain development, and failure phenomena of the tested beam specimens. Therefore, it can be used as a validated modelling framework for interpreting the mechanical

mechanisms observed in this study and for guiding future parametric studies on reinforced glulam beams. Direct application to large-span members or more complex structural systems requires additional validation considering scale effect, member slenderness, connection details, and long-term service conditions.

ACKNOWLEDGMENTS

The authors greatly appreciate the financial support from the Jiangsu Provincial Department of Housing and Urban-Rural Development Science and Technology Project (Grant Number: 2023JH01) and the 2023 Yangzhou Housing and Construction System Technology Project (Grant Number: 2023JH04). We thank The Sixth "333 High level Talent Training Project" of Jiangsu Province (Biqing Shu), Major Project of Basic Science (Natural Science) Research in Jiangsu Provincial Department of Higher Education Institutions (24KJA220004) for their funding.

Use of Generative AI

The authors declare that no AI tools were used during the writing process.

REFERENCES CITED

Anshari, B., Guan, Z. W., and Wang, Q. Y. (2017). "Modelling of Glulam beams pre-stressed by compressed wood," *Compos. Struct.* 165, 160-170. https://doi.org/10.1016/j.compstruct.2017.01.028

Anshari, B., Guan, Z. W., Kitamori, A., Jung, K., and Komatsu, K. (2012). "Structural behaviour of glued laminated timber beams pre-stressed by compressed wood," *Constr. Build. Mater.* 29, 24-32. https://doi.org/10.1016/j.conbuildmat.2011.10.002

Bedon, C., and Fragiacomo, M. (2019). "Numerical analysis of timber-to-timber joints and composite beams with inclined self-tapping screws," *Compos. Struct.* 207, 13-28. https://doi.org/10.1016/j.compstruct.2018.09.008

Chen, X., Wang, Y., Gong, Y., Ren, H., and Liu, B. (2022). "Research status of manufacture and reinforcement technology of glued laminated timber in China," *Chin. J. Wood Sci. Technol.* 36(06), 24-31,+74. https://doi.org/10.12326/j.2096-9694.2022093

De Araujo, V. (2023). "Timber construction as a multiple valuable sustainable alternative: Main characteristics, challenge remarks and affirmative actions," *Int. J. Constr. Manag.* 23(8), 1334-1343. https://doi.org/10.1080/15623599.2021.1969742

De Luca, V., and Marano, C. (2012). "Prestressed glulam timbers reinforced with steel bars," *Constr. Build. Mater* 30, 206-217. https://doi.org/10.1016/j.conbuildmat.2011.11.016

Di, J., Zuo, H., Li, Y., and Wang, Z. (2023). "Design method for glulam beams strengthened with flax fiber reinforced polymer sheets," *Structures* 49, 26-43. https://doi.org/10.1016/j.istruc.2023.01.109

EN 14080 (2013)."Timber structures — Glued laminated timber and glued solidtimber - Requirements," European Committee for Standardization, Brussels, Belgium.

Eslami, H., Jayasinghe, L. B., and Waldmann, D. (2021). "Nonlinear three-dimensional anisotropic material model for failure analysis of timber," *Eng. Fail. Anal.* 130, article 105764. https://doi.org/10.1016/j.engfailanal.2021.105764
Feng, P., Qiang, H.-l., and Ye, L.-p. (2017). "Discussion and definition on yield points of materials, members and structures," *Eng. Mech.* 34(3), 36-46. https://doi.org/10.6052/j.issn.1000-4750.2016.03.0192
Ferrier, E., Labossière, P., and Neale, K. W. (2012). "Modelling the bending behaviour of a new hybrid glulam beam reinforced with FRP and ultra-high-performance concrete," *Appl. Math. Modell.* 36(8), 3883-3902. https://doi.org/10.1016/j.apm.2011.11.062
Fossetti, M., Minafò, G., and Papia, M. (2015). "Flexural behaviour of glulam timber beams reinforced with FRP cords," *Constr. Build. Mater.* 95, 54-64. https://doi.org/10.1016/j.conbuildmat.2015.07.116
GB/T 228.1 (2022). "Metallic materials — Tensile testing — Part 1 : Method of test at room temperature," Standardization Administration of China, Beijing, China.
GB/T 15777 (2017). "Method for determination of the modulus of elasticity in compressionparallel to grain of wood," Standardization Administration of China, Beijing, China.
GB/T 1927.11 (2022). "Test methods for physical and mechanical properties of small clear wood specimens — Part11: Determination of ultimate stress in compression parallel to grain," Standardization Administration of China, Beijing, China.
GB/T 1927.14 (2022). "Test methods for physical and mechanical properties of small clear wood specimens — Part 14: Determination of tensile strength parallel to grain," Standardization Administration of China, Beijing, China.
GB/T 1927.4 (2021). "Test methods for physical and mechanical properties of small clear wood specimens — Part 4 : Determination of moisture content," Standardization Administration of China, Beijing, China.
GB/T 1927.5 (2021). "Test methods for physical and mechanical properties of small clear wood specimens — Part 5: Determination of density," Standardization Administration of China, Beijing, China.
GB 50005 (2017). "Wood structure design code," Standardization Administration of China, Beijing, China.
GB/T 50708 (2012). "Technical code of glued laminated timber structures," Standardization Administration of China, Beijing, China.
Glišović, I., Stevanović, B., and Todorović, M. (2016). "Flexural reinforcement of glulam beams with CFRP plates," *Mater. Struct.* 49(7), 2841-2855. https://doi.org/10.1617/s11527-015-0690-7
Guan, Z., Rodd, P., and Pope, D. (2005). "Study of glulam beams pre-stressed with pultruded GRP," *Comput. Struct.* 83(28-30), 2476-2487. https://doi.org/10.1016/j.compstruc.2005.03.021
Gunasekaran, P., Ghanbari-Ghazijahani, T., Valipour, H., and Alamdari, M. M. (2026). "Timber beams and columns reinforced with steel and FRP – techniques and performance: A state-of-the-art review," *Structures* 86, article 111029. https://doi.org/10.1016/j.istruc.2025.111029
He, M., Wang, Y., Li, Z., Zhou, L., Tong, Y., and Sun, X. (2022). "An experimental and analytical study on the bending performance of CFRP-reinforced glulam beams," *Front. Mater.* 8, article 802249. https://doi.org/10.3389/fmats.2021.802249

Hoffman, O. (1967). "The brittle strength of orthotropic materials," *J. Compos. Mater.* 1(2), 200-206. https://doi.org/10.1177/002199836700100210

Karagöz İşleyen, Ü., Ghoroubi, R., Mercimek, Ö., Anıl, Ö., and Tuğrul Erdem, R. (2023). "Investigation of impact behaviour of glulam beam strengthened with CFRP," *Structures* 51, 196-214. https://doi.org/10.1016/j.istruc.2023.03.038

Kliger, R., Al-Emrani, M., Johansson, M., and Crocetti, R. (2007). "Strengthening glulam beams with steel or CFRP plates," in: *Asia-PacificConf. on FRP in Structures*, Hong Kong, China, pp. 12–14.

Li, P., Ye, G., Zhou, S., Peng, T., Luo, X., and Huang, Z. (2026). "Experimental and numerical investigation into the shear performance of a novel steel-timber gusset joint," *Structures* 84, article 111038. https://doi.org/10.1016/j.istruc.2025.111038

Li, R., Chen, A., Yang, L., He, G., and Wang, H. (2025). "Experimental study on long-term performance of simply-supported glulam beams connected with steel joining plates and bolts," *Structures* 73, article 108439. https://doi.org/10.1016/j.istruc.2025.108439

Liu, H., Cui, Z., Zhao, S., Yang, S., Zhao, J., and He, F. (2025). "Elastoplastic stability analysis of semi-rigid glulam reticulated shells with bolted joints and initial imperfections," *J. Build. Eng.* 100, article 111783. https://doi.org/10.1016/j.jobe.2025.111783

Raftery, G. M., and Whelan, C. (2014). "Low-grade glued laminated timber beams reinforced using improved arrangements of bonded-in GFRP rods," *Constr. Build. Mater.* 52, 209-220. https://doi.org/10.1016/j.conbuildmat.2013.11.044

Sandhaas, C. (2012). *Mechanical Behviour of Timber Joints with Slotted-in Steel Plates*, Wöhrmann Vreden, Germany.

Shu, Z., Li, Z., He, M., Chen, F., Hu, C., and Liang, F. (2020). "Bolted joints for small and medium reticulated timber domes: experimental study, numerical simulation, and design strength estimation," *Archiv. Civ. Mech. Eng.* 20(3), article 73. https://doi.org/10.1007/s43452-020-00073-7

Soriano, J., Pellis, B. P., and Mascia, N. T. (2016). "Mechanical performance of glued-laminated timber beams symmetrically reinforced with steel bars," *Compos. Struct.* 150, 200-207. https://doi.org/10.1016/j.compstruct.2016.05.016

Tam, V. W. Y., Senaratne, S., Le, K. N., Shen, L.-Y., Perica, J., and Illankoon, I. M. C. S. (2017). "Life-cycle cost analysis of green-building implementation using timber applications," *J. Clean. Prod.* 147, 458-469. https://doi.org/10.1016/j.jclepro.2017.01.128

Thorhallsson, E. R., Hinriksson, G. I., and Snæbjörnsson, J. T. (2017). "Strength and stiffness of glulam beams reinforced with glass and basalt fibres," *Compos. Part B: Eng.* 115, 300-307. https://doi.org/10.1016/j.compositesb.2016.09.074

Uzel, M., Togay, A., Anil, Ö., and Söğütlü, C. (2018). "Experimental investigation of flexural behavior of glulam beams reinforced with different bonding surface materials," *Constr. Build. Mater* 158, 149-163. https://doi.org/10.1016/j.conbuildmat.2017.10.033

Wan, S., Xiao, H., Liu, Z., Yang, J., Yan, C., Liu, L., Zheng, X., Xie, T., Hao, C., Song, H., *et al.* (2025). "Flexural property of eco-friendly timber beams strengthened with ECC layer," *Constr. Build. Mater.* 469, article 140468. https://doi.org/10.1016/j.conbuildmat.2025.140468

Wang, Q., Wang, Z., Feng, X., Zhao, Y., and Li, Z. (2024a). "Mechanical properties and probabilistic models of wood and engineered wood products: A review of green construction materials," *Case Stud. Constr. Mater.* 21, article e03796. https://doi.org/10.1016/j.cscm.2024.e03796

Wang, Y., He, M., and Li, Z. (2024b). "Flexural behavior of glulam beams reinforced by bonded prestressing tendons," *Eng. Struct.* 315, article 118436. https://doi.org/10.1016/j.engstruct.2024.118436

Yang, C., Ling, Z., Li, Z., Qin, Z., and Shen, J. (2025). "Numerical modelling and theoretical analysis of timber-concrete glued-in threaded rod shear connectors with and without notches," *BioResources* 20(4), 10460-10486. https://doi.org/10.15376/biores.20.4.10460-10486

Yang, H., Ju, D., Liu, W., and Lu, W. J. C. (2016a). "Prestressed glulam beams reinforced with CFRP bars," *Constr. Build. Mater.* 109, 73-83. https://doi.org/10.1016/j.conbuildmat.2016.02.008

Yang, H., Liu, W., Lu, W., Zhu, S., and Geng, Q. (2016b). "Flexural behaviour of FRP and steel reinforced glulam beams: Experimental and theoretical evaluation," *Constr. Build. Mater.* 106, 550-563. https://doi.org/10.1016/j.conbuildmat.2015.12.135

Zhao, J., Liu, H., Chen, Z., Zhao, S., Yang, S., and He, F. (2024). "Investigation on the mechanical behaviour of prestressed glulam bolted joints under combined moment and axial force," *Eng. Struct.* 302, article 117487. https://doi.org/10.1016/j.engstruct.2024.117487

Article submitted: April 15, 2026; Peer review completed: May 25, 2026; Revised version received: May 31, 2026; Accepted: June 9, 2026; Published: June 22, 2026.
DOI: 10.15376/biores.21.3.7220-7246